Influence of induced magnetic fields on the static properties of Josephson-junction arrays

J. R. Phillips, H. S. J. van der Zant, J. White, and T. P. Orlando
Department of Electrical Engineering and Computer Science, Massachusetts Institute of Technology, Cambridge, Massachusetts 02139
(Received 23 September 1992)

The static properties of vortices in an array of Josephson junctions are shown to be significantly influenced by magnetic fields induced by the vortex currents. The energy barrier for vortex motion is enhanced, nearly doubling for penetration depths on the order of a cell size. Moreover, we find that correct calculation of the vortex current distribution, the magnetic moment, and the lower critical field require modeling mutual-inductance interactions between *all* cell pairs in the array. To make numerical simulation of the system feasible, an algorithm is derived that is sufficiently efficient to allow study of large (500 × 500 cells) arrays.

I. INTRODUCTION

Vortices play a central role[1] in determining the static and dynamic properties of two-dimensional (2D) superconductors. Artificially fabricated networks of superconducting islands weakly coupled by Josephson junctions are model systems to study the behavior of vortices. These arrays have also been used to study the superconducting-insulator transition, giant Shapiro steps, and the Kosterlitz-Thouless-Berezinskii (KTB) transition.

Studies of vortices in Josephson junction arrays generally neglect the magnetic fields induced by currents flowing in the array, i.e., it is assumed that the penetration depth for flux λ is much larger than the size of the array.[2] For arrays of superconductor–normal-metal–superconductor (SNS) junctions and for Al arrays of superconductor-insulator-superconductor (SIS) junctions that have been studied heretofore, this is a good approximation, especially near the KTB transition temperature. However, at lower temperatures in these systems this approximation may no longer be valid. For example, in the SNS arrays of Ref. 3 at low temperatures, λ is about 15 lattice spacings, and for some of the SIS arrays made of aluminum,[4] λ is about 5 lattice spacings at the lowest temperatures. Moreover, with the present selective niobium anodization process (SNAP) all niobium arrays have been made with λ of the order of the cell size.[5,6] The effect of induced fields must be considered for an accurate description of these systems.

Taking into account a finite λ entails solving for all the currents and fields in a self-consistent way. To our knowledge, only three numerical studies have been reported which consider the effect of induced magnetic fields (self-field effects). Nakajima and Sawada[7] studied vortex motion in a Josephson array while Majhofer, Wolf, and Dieterich[8] have investigated the magnetic behavior of 2D arrays. In both calculations, only a self-inductance term was used to describe the induced fields. Very recently, Dominguez and Jose[9] performed calculations which demonstrated that it is necessary to include nearest-neighbor mutual inductances in order to explain some of the features seen in experiments on fractional giant Shapiro steps.

Considering only self- and nearest-neighbor mutual inductances may not be sufficient to correctly determine certain vortex properties. Pearl[10] has shown that for continuous thin films of superconductor the full 3D spatial dependence of the magnetic field in the region of space outside the thin film changes the vortex structure. In particular, the effective penetration depth becomes larger and the vortex currents decay algebraically away from the center of the vortex, instead of exponentially.

In this paper, we use numerical simulation to investigate how a variety of vortex static properties are affected by finite penetration depth λ, and we calculate the self-consistent current and magnetic fields from a vortex in a 2D array. We find that in order to calculate the correct current and field distributions the full 3D behavior of the magnetic fields must be accounted for by including nearly all mutual inductance terms. However, to calculate the energy barrier for cell to cell vortex motion, which was first shown by Lobb, Abraham, and Tinkham (LAT)[2] to be $0.2E_J$, where E_J is the Josephson coupling energy, including only self- and nearest-neighbor inductances is sufficient. The LAT calculation neglected induced magnetic fields. We show that induced fields may increase the energy barrier substantially above $0.2E_J$. Our calculations also show that the thermodynamic lower critical field of the array is enhanced when the computation self-consistently accounts for induced magnetic fields; and that by using only a self-inductance term to model the induced fields the lower critical field is overestimated.

Self-consistently determining the currents and fields in a Josephson-junction array is a difficult numerical problem as the fields induced by a junction current affect the current through every junction in the array. This dense interaction implies that for an array having N cells, on

the order of N^2 words of computer memory are required just to store the mutual inductance matrix, and if a direct approach is used to compute the self-consistent solution by factoring the inductance matrix,[11] on the order of N^3 operations are required. For example, the inductance matrix of a 100×100 array requires more than 400 megabytes of memory to store and on the order of 10^{12} operations to factor.

To make the computation tractable, we derive a simulation algorithm which combines several numerical techniques with an appropriate problem formulation. When used to simulate an N-cell array, this approach reduces the storage required to order N and reduces the computation time to order $N \log N$, making it possible to compute self-consistent array currents and fields in a 100×100 array in a minute or so using a scientific workstation (IBM RS6000).

In Sec. II we present a method for analysis of general networks of Josephson junctions, an example of which is the square array. In Sec. III we discuss the calculation of the inductances which describe the magnetic interactions in the array. Section IV contains a description of the numerical algorithm we use to analyze the array, and we present the results of our calculations in Sec. V.

II. MESH ANALYSIS OF THE JOSEPHSON NETWORK

In this section, we describe the analysis of networks consisting of Josephson junctions. First we discuss the specific example of a square Josephson-junction array. Next, using the principles and compact notation of basic circuit theory,[12] we present a method of analysis which can be applied to very general networks.

The first state variables for the Josephson network are the gauge-invariant phase differences ϕ across each junction in the network. The directed sum of the junction phase differences around a loop[13] is then related to the amount of flux Φ passing through the loop by[7,8]

$$\sum \phi = -2\pi \frac{\Phi}{\Phi_0} + 2\pi n \tag{1}$$

where n is an integer and Φ_0 is a flux quantum. For example, in the square array, each array cell can be associated with a loop, or *mesh*, as shown in Fig. 1, where the field is taken to be positive out of the paper. Equation (1) is applied to each mesh in the array so that

$$-\phi^x_{i,j+1} - \phi^y_{i,j} + \phi^x_{i,j} + \phi^y_{i+1,j} = -2\pi \frac{\Phi_{i,j}}{\Phi_0} + 2\pi n_{i,j} \ . \tag{2}$$

The *branch* (junction) currents, $I^\alpha_{i,j}$ in Fig. 1 ($\alpha = x$ or y), can be related to mesh currents I^m circulating in each loop previously defined by the phase loop sum, Eq. (2). For the square array, at mesh (i,j)

$$I^x_{i,j} = I^m_{i,j} - I^m_{i,j-1}, \tag{3a}$$

$$I^y_{i,j} = I^m_{i-1,j} - I^m_{i,j}. \tag{3b}$$

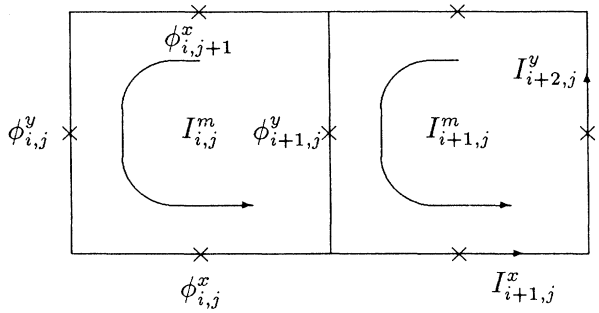

FIG. 1. A possible network indexing for the square Josephson array.

Since any mesh current entering a node also leaves it, by expressing the branch currents in this form we insure that the requirement of current conservation is identically satisfied at each node of the network. For Josephson junctions the branch currents are related to the gauge-invariant phase differences by

$$I^x_{i,j} = I_c \sin \phi^x_{i,j}, \tag{4a}$$

$$I^y_{i,j} = I_c \sin \phi^y_{i,j}, \tag{4b}$$

where I_c is the single-junction critical current.

For convenience, the flux is split into two parts,

$$\Phi = \Phi^{\text{ext}} + \Phi^{\text{ind}}_{i,j}, \tag{5}$$

where Φ^{ext} is due to an externally applied field, and $\Phi^{\text{ind}}_{i,j}$ is the flux through the cell (i,j) induced by the currents in the array. With the usual identification $\Phi^{\text{ext}}/\Phi_0 = f$, Eq. (2) becomes

$$-\phi^x_{i,j+1} - \phi^y_{i,j} + \phi^x_{i,j} + \phi^y_{i+1,j} + 2\pi \frac{\Phi^{\text{ind}}_{i,j}}{\Phi_0} = 2\pi(n_{i,j} - f) \ . \tag{6}$$

The induced flux $\Phi^{\text{ind}}_{i,j}$ in each mesh is calculated by defining the inductance $L_{i,i',j,j'}$ such that a mesh current $I^m_{i',j'}$ induces a flux $L_{i,i',j,j'} I^m_{i',j'}$ in mesh (i,j). Thus

$$\Phi^{\text{ind}}_{i,j} = \sum_{i',j'} L_{i,i',j,j'} I^m_{i',j'} \ . \tag{7}$$

The factor $L_{i,i',j,j'}$ is usually referred to as the mutual inductance between mesh (i,j) and (i',j'), while $L_{i,i,j,j}$ is the self-inductance of mesh (i,j). We defer the actual calculation of the inductances to Sec. III.

Equations (3), (4), (6), and (7) constitute a system of nonlinear equations which can be solved for the junction phase differences and mesh currents in the square array. These equations can be written more compactly by introducing the matrix M which represents the loop-sum operator defined by Eq. (2). Writing the phase differences ϕ as a single vector quantity, Eq. (6) becomes

$$M\phi + 2\pi \frac{\Phi^{\text{ind}}}{\Phi_0} = 2\pi(n - f) \tag{8}$$

where n is now a vector quantity. We let the vector I_b denote the branch currents $I^{\alpha}_{i,j}$ ($\alpha = x$ or y), and the vector I_m the mesh currents $I^{m}_{i,j}$. The general form of the relation between branch and mesh currents, which is Eq. (3) in the case of the square array, can be shown to be[12]

$$M^T I_m = I_b \ . \tag{9}$$

Equation (4) in the vector notation is

$$I_b = I_c \sin\phi \ , \tag{10}$$

while the mesh currents and induced fluxes are related by [Eq. (7)]

$$\Phi^{\rm ind} \equiv L I_m \ . \tag{11}$$

Thus the diagonal elements of L are the self-inductances, and the off-diagonal elements are the mutual inductances. Combining Eqs. (8)–(11) yields a set of equations to describe the Josephson array

$$M\phi + \frac{2\pi}{\Phi_0} L I_m = 2\pi(n-f), \tag{12a}$$

$$M^T I_m = I_c \sin\phi \ . \tag{12b}$$

Note that the branch current vector I_b has been eliminated as an unknown.

Scaling all currents in units of I_c, all lengths in units of the lattice constant p, and defining $\Lambda \equiv L/\mu_0 p$, Eq. (12) becomes

$$M\phi + \frac{1}{\lambda_\perp} \Lambda I_m = 2\pi(n-f), \tag{13a}$$

$$M^T I_m = \sin\phi, \tag{13b}$$

where $\lambda_\perp$, given by

$$\lambda_\perp = \frac{\Phi_0}{2\pi\mu_0 I_c p} \tag{14}$$

is the effective dimensionless penetration depth for a 2D system.[14] It should be emphasized that the above approach to deriving a system of equations applies to general Josephson networks, not just square arrays, and that all self-field effects have been included.

As an approximation to the full inductance matrix L, we may be interested in the case where only the self-inductance of each cell is retained when calculating the induced fields. In that event, we may also write the equations for the Josephson network in a suggestive form. Including only the self-inductance L_0 of the meshes when calculating the induced fields corresponds to retaining only the diagonal entries of L. When only the self-inductance is retained, the appropriate penetration depth is the usual Josephson penetration depth for the array, λ_J, which is given in its dimensionless form by[15]

$$\lambda_J^2 = \frac{\Phi_0}{2\pi L_0 I_c} \ . \tag{15}$$

For this special case, the general system of Eq. (13) can be written as

$$M\phi + \frac{1}{\lambda_J^2} I_m = 2\pi(n-f), \tag{16a}$$

$$M^T I_m = \sin\phi \ . \tag{16b}$$

III. COMPUTING THE INDUCTANCE MATRIX

In this section we describe the computation of the elements of the inductance matrix L defined in Eq. (11). In general, to compute $\Phi^{\rm ind}_{i,j}$ in each mesh, the gauge $\nabla \cdot \mathbf{A} = 0$ is chosen so that the vector potential can be computed from the current density by

$$\mathbf{A}(\mathbf{r}) = \frac{\mu_0}{4\pi} \int \frac{\mathbf{J}(\mathbf{r}')d^3r'}{|\mathbf{r}-\mathbf{r}'|} \ . \tag{17}$$

We could in principle extract an inductance for arbitrary superconducting structures by self-consistently computing the current distribution due to an induced phase difference. The flux through each mesh is then computed from the vector potential $\mathbf{A}$ given by Eq. (17). For simplicity, we approximate the inductance matrix with that generated by a normal metal with regions of constant current density.[16] In this approximation the current-carrying portions of the array can be decomposed into a set of rectangular bars, each carrying a constant current.[17]

To see why this is a reasonable assumption, consider an actual array geometry,[18,6] as pictured in Fig. 2. The Josephson array consists of two layers of superconducting islands, one lying above the other, with the junctions occurring at the overlap of a top-layer island with a bottom-layer island. Typically the vertical dimensions of the islands are considerably less than the lattice spacing p. The current in each bar is the current through the junction geometrically located at the center of the bar. The approximate geometry is shown in Fig. 3. Each bar is associated with a branch in the circuit, and the requirement of no net current flowing into each island is achieved by enforcing current conservation at the nodes of the equivalent circuit formed by the bars. Thus the current density $\mathbf{J}(\mathbf{r})$ can be computed from the branch currents, which are in turn computed from the mesh cur-

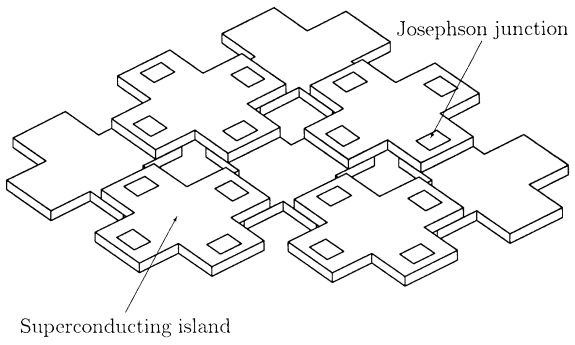

FIG. 2. The physical Josephson array. Junctions occur at overlap of the islands.

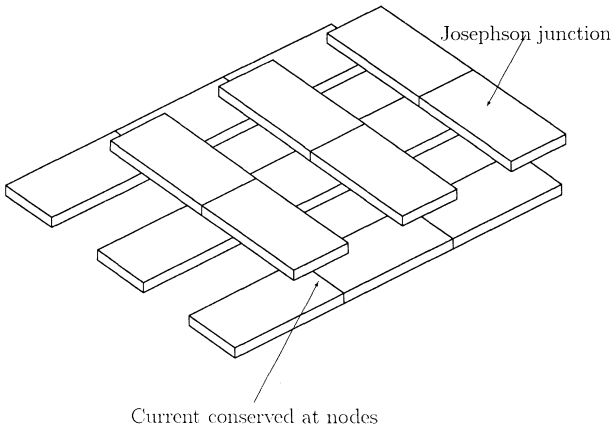

FIG. 3. Approximate geometry for calculation of the inductance matrix. The junctions are considered to lie in the center of the bars. Current conservation is enforced at the points where four bars meet, which corresponds to the superconducting islands of Fig. 2.

rents through use of Eq. (9). The induced flux $\Phi_{i,j}^{\rm ind}$ given by $\int \mathbf{A}\cdot d\mathbf{l}$ around the loop defining the mesh is therefore a unique linear function of the mesh currents. In this paper, we assume bars with dimensions of length p, width $0.5p$, and thickness $0.02p$, where p is the lattice constant for the square array, which is typical for fabricated SIS arrays.[18,6]

For an arbitrary loop, we can compute the flux through the loop by computing $\int \mathbf{A}\cdot d\mathbf{l}$ along each branch (bar) in the loop, and then summing over the loop's component branches. To account for each bar's finite cross section, we average $\int \mathbf{A}\cdot d\mathbf{l}$ over the cross-sectional area a_n, so that

$$\Phi_{i,j}^{\rm ind} = \sum_{n\in<i,j>} \frac{1}{a_n}\int_n \mathbf{A}\cdot d\mathbf{l}\, da_n \tag{18}$$

where the summation index $n \in \langle i,j\rangle$ indicates all those branches in the mesh (i,j). The vector potential is then given by

$$\mathbf{A}(\mathbf{r}) = \sum_k \frac{\mu_0}{4\pi}\frac{I_k}{a_k}\int \frac{d\mathbf{l_k}\, da_k}{|\mathbf{r}-\mathbf{r_k}|}, \tag{19}$$

where I_k is the branch current associated with bar k and the sum k runs over all the bars in the array. Thus,

$$\frac{1}{a_n}\int_n \mathbf{A}\cdot d\mathbf{l}\, da_n = \sum_k L_{nk}^b I_k \tag{20}$$

with the branch inductances L^b given by

$$L_{nk}^b = \left[\frac{1}{a_k a_n}\frac{\mu_0}{4\pi}\int \frac{d\mathbf{l_k}\cdot d\mathbf{l_n} da_n da_k}{|\mathbf{r_n}-\mathbf{r_k}|}\right] . \tag{21}$$

In evaluating the L_{nk}^b, we distinguish three cases. For $n=k$, the presence of the singularity makes it advisable to treat the integral analytically. Expressions are available in the literature[17] for the integral of Eq. (21) when $n=k$. For large $|r_n - r_k|$ it is sufficient to assume that the current is carried by filaments of vanishing cross section, so that the integral is easily performed analytically. For $n \neq k$, but small $|r_n - r_k|$, the integral in Eq. (21) is computed numerically. In this paper, we have used the filament approximation when the distance between bar centers is more than $5p$.

Combining Eqs. (18) and (20), the induced flux in mesh (i,j) can be written as

$$\Phi_{i,j}^{\rm ind} = \sum_{n\in<i,j>}\sum_k L_{nk}^b I_k, \tag{22}$$

where the I_k are the branch currents. In the vector notation Eq. (22) becomes

$$\Phi^{\rm ind} = ML^bI_b = ML^bM^TI_m \tag{23}$$

and thus

$$L = ML^bM^T \tag{24}$$

with the elements of L^b defined in Eq. (21).

IV. NUMERICAL METHOD

In this section we describe the numerical method used to solve the nonlinear system of Eq. (13). The nonlinear system is solved by Newton's method, which gives rise to a sequence of linear systems of equations. To solve the linear systems we use an iterative method, the generalized minimal residual (GMRES) algorithm.[19] Each iteration of the GMRES algorithm requires a dense matrix-vector product whose cost is reduced by using the fast Fourier transform (FFT). Finally the convergence of GMRES is accelerated by an FFT-based preconditioner. As the computational cost of the final algorithm grows essentially as $N\log N$, where N is the number of cells in the array, we have been able to study relatively large arrays.

A. Newton's method

Newton's method[20] to solve the nonlinear system $f(x)=0$ consists of the repeated iteration

$$J(x^k)\delta x^k = -f(x^k) \quad \text{with} \quad x^{k+1} = x^k + \delta x^k \tag{25}$$

where J is the Jacobian matrix,

$$J_{ij}(x^k) = \left.\frac{\partial f_i}{\partial x_j}\right|_{x^k} \tag{26}$$

and the superscript k indicates evaluation of a quantity at iteration k. The iteration is terminated when $||f(x^k)||$, the norm of the residual, is sufficiently small. By defining

$$f_1(I_m,\phi) = M\phi + \frac{1}{\lambda_\perp}\Lambda I_m - 2\pi(n-f), \tag{27a}$$

$$f_2(I_m,\phi) = M^TI_m - \sin\phi, \tag{27b}$$

then if $f_1(I_m,\phi)=0$ and $f_2(I_m,\phi)=0$, I_m,ϕ will be

the solution to Eq. (13). Applying Newton's method to solving Eqs. (27a) and (27b) leads to the iteration

$$\begin{bmatrix} M & \frac{1}{\lambda_\perp}\Lambda \\ -C & M^T \end{bmatrix} \begin{bmatrix} \delta\phi^k \\ \delta I_m^k \end{bmatrix} = - \begin{bmatrix} f_1^k \\ f_2^k \end{bmatrix}, \tag{28}$$

$$\phi^{k+1} = \phi^k + \delta\phi^k, \quad I_m^{k+1} = I_m^k + \delta I_m^k, \tag{29}$$

where the matrix C in the Jacobian is diagonal with entries given by

$$C_{ii} = \cos\phi_i^k. \tag{30}$$

Assuming C is invertible, we can simplify the system by using block Gaussian elimination to eliminate the variable $\delta\phi$ in Eq. (28). The new system of equations is

$$\left(MC^{-1}M^T + \frac{1}{\lambda_\perp}\Lambda\right)[\delta I_m] = -[f_1 + MC^{-1}f_2] \tag{31}$$

which by defining

$$\tilde{J} \equiv \left(MC^{-1}M^T + \frac{1}{\lambda_\perp}\Lambda\right) \quad \text{and} \quad \tilde{f} \equiv -[f_1 + MC^{-1}f_2] \tag{32}$$

becomes

$$\tilde{J}\,\delta I_m = \tilde{f}\ . \tag{33}$$

Since C is diagonal, it will be invertible if $\cos\phi_i \neq 0$ for all i, which may not be the case. We insure invertibility of C by modifying its entries to be bounded away from zero. Such a scheme of approximating the Jacobian may affect the convergence of Newton's method but the computed solution will still be accurate if the iteration is repeated until f_1 and f_2 are small enough.

B. Solution of the linear system

Although it is possible to form $\tilde{J}$ of Eq. (33), and then factor $\tilde{J}$ using Gaussian elimination, this is an impractical approach for even moderately sized arrays, because the memory and computational requirements grow too rapidly with problem size. Instead, an iterative procedure which uses an implicit representation of $\tilde{J}$ can dramatically reduce storage and computational cost.

One such iterative procedure for solving Eq. (33) is the GMRES algorithm.[19] The GMRES algorithm to solve the general linear system $Ax = b$ constructs a series of approximations $x^0, x^1, \ldots, x^k$ to the solution x. At each iteration GMRES selects the approximation x^k from the space spanned by the vectors $\{r^0, Ar^0, A^2r^0, \ldots, A^{k-1}r^0\}$ in order to minimize the norm of the residual $||r^k||$, where the residual is defined by $r^k = b - Ax^k$. The algorithm is terminated when the norm of the residual, $||r^k||$, is less than some tolerance $||r||_{\min}$.

The key step in each GMRES iteration is the computation of a matrix-vector product, Ax^k. As the matrix $\tilde{J} = [MC^{-1}M^T + (1/\lambda_\perp)\Lambda]$ is dense, a direct matrix-vector product requires $O(N^2)$ operations. However, for the regular arrays considered in this paper, the elements of the inductance matrix Λ are a function only of relative cell positions. That is, in terms of the $L_{i,i',j,j'}$ defined by Eq. (7)

$$L_{i,i',j,j'} = L_{|i-i'|,|j-j'|}\ . \tag{34}$$

Thus the operation of forming the product $\Lambda \times x^k$ is simply a 2D linear discrete convolution, which can be performed in $O(N \log N)$ operations by use of the FFT.[21] Note that because in this paper we use free space boundaries (and thus no periodicity of any variable is enforced) zero-padding techniques are required to obtain a linear convolution. The remaining part of $\tilde{J}$, $MC^{-1}M^T$, is sparse so the product $MC^{-1}M^Tx^k$ is inexpensive to compute directly. Furthermore, when the FFT is used to compute the matrix-vector product, the cost of computing the dense part (Λ) of the product is comparable to the cost of computing the sparse part ($MC^{-1}M^T$), so that there is no computational advantage to neglecting the mutual inductances of distant cells.

C. Accelerating GMRES convergence

After completing k iterations, the GMRES algorithm as discussed in Sec. IV B requires $O(kN \log N)$ operations to compute the matrix-vector products, and $O(k^2N)$ operations to construct an approximate solution to the linear system (see Ref. 19 for details of the cost of GMRES). Thus it is essential to minimize the number of iterations k.

We can improve the convergence of GMRES by applying it to the preconditioned problem

$$APy = b \quad \text{where} \quad y = P^{-1}x \tag{35}$$

where we solve for y and then calculate $x = Py$. If $P \simeq A^{-1}$ then AP will be close to the identity matrix I and convergence of GMRES will be rapid. To be an effective preconditioner, P must also be easy to compute. In order to choose P, first note that the dominant terms in Λ must be the self- and nearest-neighbor inductances. This can be seen by noting that the physical interpretation of the entry Λ_{ij} of Λ is the amount of flux through loop i produced by a current in loop j. Thus, the off-diagonal entries Λ_{ij} are generally negative and decay as $1/r^3$, r being the distance between the loops, while the diagonal self-inductances Λ_{ii} are positive. It is useful to know that, assuming $\Lambda_{ii} > 0$ and $\Lambda_{ij} < 0$, which is the case for the geometry considered in this paper, then by conservation of magnetic flux, each diagonal element of Λ is greater than the sum of the magnitudes of the off-diagonal elements in the same row, that is

$$\Lambda_{ii} > \sum_j |\Lambda_{ij}| \tag{36}$$

and thus Λ is positive definite. Secondly, the entries of C^{-1} enter the matrix $\tilde{J} = MC^{-1}M^T + (1/\lambda_\perp)\Lambda$ at the positions occupied by the self- and nearest-neighbor inductances. When the currents in the array are not large (few vortices and small applied fields), C^{-1} is approximately the identity matrix I. Defining $\tilde{\Lambda}$ to be the part of Λ corresponding to self- and nearest-neighbor induc-

tances, the preconditioning matrix is given by

$$P^{-1} = MIM^T + \frac{1}{\lambda_\perp}\tilde{\Lambda} \ . \tag{37}$$

Clearly P^{-1} is also positive definite. For the square array, P^{-1} has the same form as the matrix arising from a five-point finite-difference discretization on a uniform mesh of the Poisson equation with Dirichlet boundary conditions. It is well known that for a matrix of this form, Px can be computed by use of sine transforms.[22] If the size of the array in one direction is one less than the product of small primes, this operation can be made very fast by the use of fast sine transforms.

D. Final algorithm

We present below the final algorithm for solving Eq. (13).

Set $k = 0$
guess I_m^0, ϕ^0
Compute the Newton residual, f_1^0 and f_2^0
repeat {
  Compute $\tilde{J}, \tilde{f}$ from Eqs. (30), (32)
  Set $j = 0$
  Set $||r_{\min}|| = \gamma||\tilde{f}||$
  guess $y^0 = 0$
  repeat {
    Set $j = j + 1$
    Choose y^j to minimize $||r^j||$
    Compute the residual, $r^j = \tilde{f} - \tilde{J}Py^j$:
      —use FST to compute $P \times y^j$
      —use FFT in computing $\tilde{J} \times (Py^j)$
  } until $||r^j|| < ||r||_{\min}$
  Set $\delta I_m^k = Py^j$
  Compute $\delta\phi^k$ from δI_m^k using Eq. (28)
  Set $\phi_{k+1} = \phi^k + \delta\phi^k$
  Set $I_m^{k+1} = I_m^k + \delta I_m^k$
  Compute the Newton residual, f_1^k and f_2^k
} until $||f_1^k|| < \epsilon$ and $||f_2^k|| < \epsilon$
Return (I_m^k, ϕ^k) as the solution

Two parameters, ϵ and γ, deserve note. First, ϵ, the tolerance for convergence of the Newton iteration, controls the accuracy of the computed solution and is generally chosen in the range $10^{-4} - 10^{-6}$. The parameter γ links how accurately the Newton iterates are computed to how close the Newton iteration is to convergence.[23,24] Earlier Newton iterations do not require precise solutions of the linear system, so $||r_{\min}||$ is chosen to be large then, hopefully reducing the time spent solving linear systems and reducing the overall computational effort. In this paper, we have generally chosen $\gamma = 0.05$.

The algorithm's efficiency makes simulation of large arrays (up to 10^5 cells) possible using a typical scientific workstation. We have found that each Newton iteration requires only 10–20 GMRES iterations to solve the linear systems, and indeed the computation time is empirically observed to grow as $N \log N$ with N being the number of cells in the array.

V. RESULTS AND DISCUSSION

We have calculated single-vortex solutions to Eq. (13) in arrays of sizes ranging from 31 × 31 cells to 511 × 511 cells, with $\lambda_\perp$ ranging from 0.5 to infinity (no self-field effects). As an initial guess to the single-vortex solution, we use the "arctan approximation" (as discussed for example in Ref. 2) to obtain a value for the phase of the order parameter at each superconducting island. The initial guess for the junction phase differences ϕ is obtained by differencing the initial island phases. In all cases the arrays are taken to have free-space boundary conditions. In this paper we present mostly results from study of an array of 127 × 127 cells, which is typical for fabricated arrays of SIS junctions. All the calculations described here were performed on an IBM RS6000/540 workstation, using the C programming language. On this system, finding a single-vortex solution in a 127 × 127 array requires about 90 CPU seconds.

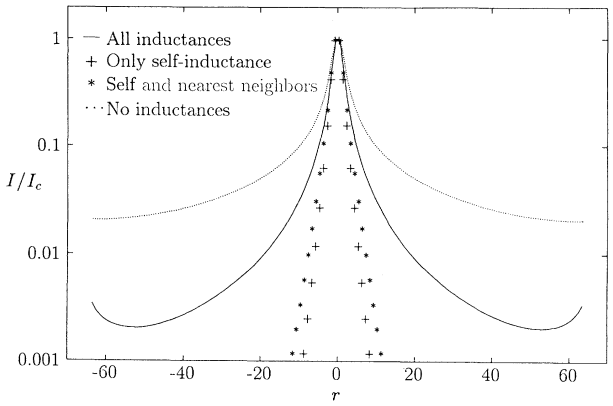

FIG. 4. Currents for a single vortex in a 127 × 127 cell Josephson array, with $\lambda_\perp = 2.0$.

A. Single-vortex solution

We first consider the calculation of the current distribution produced by a single vortex located in the center cell of a square 127 × 127 cell Josephson array. To demonstrate the influence of the self-field effects, we have taken $\lambda_\perp = 2.0$. Figure 4 shows the computed junction currents along a cross section taken through the center array cell, parallel to one of the edges, as a function of r, the distance of the junction from the array center, in units of the lattice spacing p.

We have computed the junction currents using four different assumptions about the self-fields: (1) neglecting induced fields altogether (i.e., taking $\lambda_\perp \to \infty$), (2) including only self-inductance terms in L, (3) including only self- and nearest-neighbor inductances, and (4) including all the terms in L. In interpreting these results, it is useful to consider analogies with a continuous superconductor.

In the limit $\lambda_\perp \to \infty$, we expect that a good description of the vortex statics is given by the "arctan approximation" where the current decays as $1/r$ away from the core. The calculated vortex current in this limit is shown as the dotted line in Figure 4. We have confirmed that the current decay has the correct asymptotic form.

A decay of the current away from the core faster than $1/r$ can be taken as indicative of self-field effects. The first approximation to the self-field effect is the inclu-

sion of a self-inductance term. In this model, the current circulating in each cell induces flux only in that cell. Assuming that the self-fields may be described by only a self-inductance coefficient is equivalent to assuming that the magnetic field is directed normal to the plane of the array. Thus, the appropriate continuum analog of the Josephson array with induced fields modeled by only a self-inductance term is a 3D bulk superconductor. In this case, it is well known that the London vortex solution for the current density has the form

$$J(r) = \frac{\Phi_0}{2\pi\mu_0\lambda_L^3} K_1(r/\lambda_L) \tag{38}$$

with K_1 the modified Bessel function of the second kind and λ_L the London penetration depth. For $r \gg \lambda_L$, $J(r) \sim \exp(-r/\lambda_L)/\sqrt{r}$. When the currents in the array are computed using only the self-inductance in L, shown as the crosses in Fig. 4, the current falls off roughly exponentially, as expected. Assuming the current $I(r)$ of the form $I(r) \simeq \exp(-r/\lambda)/\sqrt{r}$, where $r \gg \lambda$, and neglecting the junctions near the core and near the edge, we have extracted λ from the computed solution. We have found that $\lambda = \lambda_J$ within a few percent, confirming that λ_J is the appropriate penetration depth for the Josephson array with induced fields described only by a self-inductance term.

The next level of approximation of the induced fields is to include nearest-neighbor mutual inductance terms in addition to the self-inductance. As shown by the starred points of Fig. 4, the addition of the nearest-neighbor inductances does not substantially alter the form of the current solution. In particular, the current still falls off exponentially away from the core.

Neglect of self-fields and inclusion of only the self-inductance result in vortex current profiles which represent two limiting cases: slow algebraic and exponential, respectively. For a physically correct model, our calculations suggest that all the mutual inductances need to be included. The solid line solution plotted in Fig. 4 shows the vortex currents in this case. If all the mutual inductances are retained, the appropriate continuum analog is a thin film. The solution to the London equations for a vortex in an infinite thin film has been obtained by Pearl,[10] who has shown that the surface current K_s of a vortex in an infinite thin film can be written in the approximate form

$$K_s(r) = \frac{\phi_0}{2\pi\mu_0\lambda_\perp^2} \frac{1}{(r/\lambda_\perp)[1 + (r/2\lambda_\perp)]} \tag{39}$$

which has the form $K_s \sim 1/r^2$ for $r \gg \lambda_\perp$. Thus when all mutual inductances are included, we expect the currents to have a slower algebraic decay, as contrasted with the fast exponential fall off observed when only the self-inductance is retained. The solid-line plot in Fig. 4 demonstrates this slower decay. Away from the boundaries, we have confirmed the asymptotic $1/r^2$ decay expected from the continuum limit.

The difference between the forms of the solutions with algebraic and exponential decay occurs because, in the language of continuous superconductors, including only the self-inductance is mathematically equivalent to the case of the 3D bulk superconductor, where the field is only in one direction, parallel to the core. In an actual array, the magnetic field is free to penetrate the free space above and below the array. When the induced fields are described only by a self-inductance term, the field lines cannot "turn around" in the space above the array, which results in a stronger screening effect.

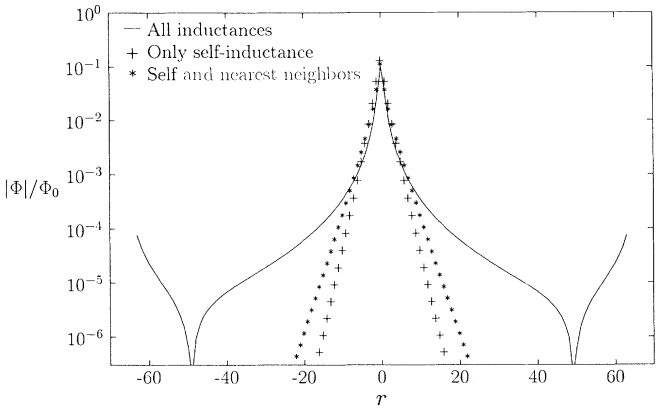

FIG. 5. Magnitude of the magnetic flux of a single vortex in a 127×127 cell Josephson array. Note the sign change that occurs at $r \simeq 50$.

When all the mutual inductances are included in the problem, the solution displays an additional feature. The current decreases away from the vortex core, but then rises near the edge of the array. In order to understand this effect, consider Fig. 5 which shows the magnitude of the flux through each cell along the same array cross section as in Fig. 4. When all the mutual inductances are included in the problem, the flux undergoes a sign change near the edge of the array. A mesh current induces a positive flux through itself, via the self-inductance, but a *negative* flux through far-away meshes, via the mutual inductances. In other words, the mutual inductances represent the "turning-around" of the lines of magnetic flux, and thus the field outside the array must be of opposite sign, as is the field near the edge. Since the flux has changed sign near the edge, the current must increase. In contrast, when only the self-inductance is included, the field is forced to zero at the edge of the array. We emphasize that the sign change of the flux is a result intrinsic to both the finite sample size and the inclusion of the full set of mutual inductances. The sign change of the flux is also present in a thin film of continuous superconductor, as shown in the Appendix where we solve the appropriate integral form of the London equations in a disk.

Numerical simulation of the array with all mutual inductances included reveals that the commonly used method of images solution is, strictly speaking, invalid for thin films and 2D arrays. We might attempt to approximate the solution to the Josephson array vortex by using the continuum limit solution. Image vortices from an infinite film solution could be placed to account for finite boundaries, as would be done for a finite sample of bulk superconductor. If the image solution were valid, we would expect the slope of the current to go to zero at the edge (as it does when no self-fields are included in

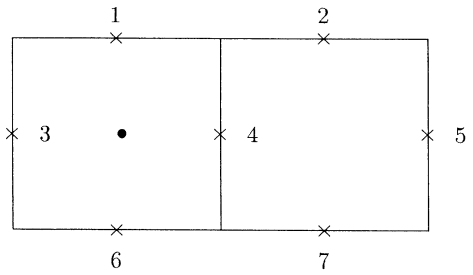

FIG. 6. Junctions used for the estimate of the energy barrier ΔE. The vortex is centered at the dot (•) for the calculated of E_{center} and on junction 4 for the calculation of E_{junction}.

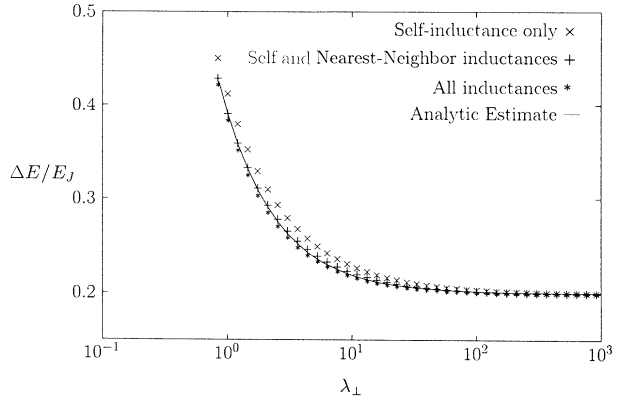

FIG. 7. Cell-cell energy barrier ΔE in units of the Josephson energy, as a function of $\lambda_\perp$ in a 127 × 127 cell Josephson array.

the problem). However, when all mutual inductances are included the computed solution is qualitatively different, as the current rises and the flux changes sign near the edge.

B. Energy barrier

We next consider a generalization of the energy barrier calculation first performed by Lobb, Abraham, and Tinkham.[2] This calculation considered the energy difference ΔE between a vortex centered in a cell, and a vortex centered on a junction, as shown in Fig. 6. ΔE was taken to be the barrier for cell-to-cell motion of the vortex. The original calculation was performed in the no self-field limit, $\lambda_\perp \to \infty$, and the relevant energy was strictly the Josephson supercurrent energy

$$E_s = \sum E_J(1-\cos\phi) \ . \tag{40}$$

The calculated energy barrier was found to be $\Delta E \simeq 0.2E_J$ for a large square array.

We have performed a similar calculation in the 127 × 127 array, where we have accounted for self-field effects so that the magnetic energy E_m must be included in the energy $E = E_s + E_m$. For a system of current loops $E_m = \frac{1}{2}\sum_{i,j} I_i L_{ij} I_j$, where L_{ij} is the mutual inductance between loops i and j, with currents I_i and I_j flowing in them. In units of the Josephson coupling energy, $E_J = I_c\Phi_0/2\pi$, the magnetic energy can be written as the vector dot product

$$E_m = \frac{1}{2\lambda_\perp} I_m^T \Lambda I_m \ . \tag{41}$$

Figure 7 shows the calculated energy barrier ΔE, expressed in units of E_J as a function of $\lambda_\perp$. In the limit $\lambda_\perp \to \infty$, we obtain $\Delta E = 0.199E_J$, in agreement with the LAT calculation. The energy barrier increases as $\lambda_\perp$ decreases, which is a result of the increased localization of the vortex by the self-field effect. We note that including all the mutual inductances has a relatively small effect on this calculation. As can be seen from the crosses in Fig. 7, a nearest-neighbor approximation of the full inductance matrix gives good results. This is not surprising, since we expect that properties of the vortex which depend most strongly on the structure of the vortex near the core will be less affected by the inclusion of the mutual inductances, while properties that are related to longer length scales or the finite size of the array (such as the effects of applied fields and currents) will be more strongly affected.

A very simple model gives a good description of the effect of self-fields on the energy barrier. It is reasonable to assume that the major differences between a vortex centered in a cell and a vortex centered on a junction half a lattice spacing away occur near the vortex centers. We assume that the junction phase differences near the vortex center are accurately described by the "arctan approximation." Consider a vortex in the center of a cell, as shown in Fig. 6. For purposes of the energy barrier calculation, we assume that the energy is due to the Josephson energy of junctions 1, 3, 4, and 6, plus the magnetic energy due to the circulating current in the cell.

$$E_{\text{center}} = E_J(4-\cos\phi_1-\cos\phi_3-\cos\phi_4-\cos\phi_6)+\tfrac{1}{2}LI^2 \tag{42}$$

where L is the self-inductance of the cell. In the "arctan approximation" the phase differences are all $\pi/2$ so that the circulating current is I_c. Thus the energy for the vortex centered in a cell is

$$E_{\text{center}} = 4E_J + \tfrac{1}{2}LI_c^2 \ . \tag{43}$$

In the high-energy state, the vortex is centered directly on the junction labeled 4 in Fig. 6. To calculate the energy of this configuration, we consider the magnetic energy due to the self-inductance of both cells, the magnetic energy due to mutual inductance between the cells, and the Josephson energy of junctions 1, 2, 4, 6, and 7. This yields

$$E_{\text{junction}} = E_J(5-\cos\phi_1-\cos\phi_2-\cos\phi_4-\cos\phi_6-\cos\phi_7)+\tfrac{1}{2}LI_1^2+\tfrac{1}{2}LI_2^2+MI_1I_2 \tag{44}$$

as an approximation to the energy for the on-junction vortex, where I_1 and I_2 are the circulating currents in the two cells and M is the mutual inductance between the cells. The "arctan approximation" gives π for the phase difference of junction 4, and arctan(2) for the phase difference of the other junctions (junctions 1, 2, 6, and 7). The circulating currents must then be $I = I_1 = I_2 = 2I_c/\sqrt{5}$, so the energy E_{junction} of the on-junction vortex is

$$E_{\text{junction}} = E_J\left(2 + 4\cos\frac{1}{\sqrt{5}}\right) + 0.8LI_c^2 + 0.8MI_c^2 \tag{45}$$

and the energy barrier $\Delta E = E_{\text{junction}} - E_{\text{center}}$ is

$$\Delta E = 0.211E_J + 0.3LI_c^2 + 0.8MI_c^2 \ . \tag{46}$$

Expressing the result in terms of the Josephson penetration depth λ_J, the energy barrier is approximately given by

$$\frac{\Delta E}{E_J} = 0.2\left[1 + \frac{3}{2}\frac{1}{\lambda_J^2}\left(1 + \frac{8}{3}\frac{M}{L}\right)\right] \ . \tag{47}$$

The solid line of Fig. 7 shows the analytic approximation to the energy barrier, Eq. (47). The agreement with the numerical calculation is surprisingly good.

The form of Eq. (47) tempts us to define an effective penetration depth that accounts for the nearest-neighbor inductances

$$\lambda_{\text{eff}}^2 = \frac{\lambda_J^2}{1 + \frac{8}{3}\frac{M}{L}} \ . \tag{48}$$

If we assume a form $J(r) \sim e^{-r/\lambda}$ for the vortex currents calculated in Sec. V A when self- and nearest-neighbor inductances are included, we find that λ_{eff} predicts λ within about twenty percent (note that $M < 0$, so the inclusion of the nearest-neighbor inductances increase the effective penetration depth).

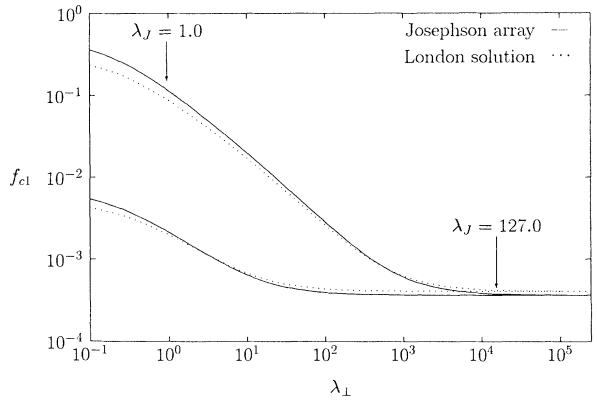

FIG. 8. f_{c1} in a 127 × 127 cell Josephson array. The upper solid curve shows f_{c1} in an array calculated using only a self-inductance term to describe the self-fields, while the lower solid curve shows f_{c1} calculated using all mutual inductances. The upper and lower dotted lines show f_{c1} calculated using London's equations in a infinite cylinder and thin disk, respectively.

C. Thermodynamic lower critical field

The applied frustration (field) f_{c1} necessary for a vortex solution in the array to be energetically favorable is strongly affected by self-fields. To calculate f_{c1}, we calculate the energy of an array containing one vortex in an applied field, E_V, and the energy of a vortex in a Meissner-like state with no vortex present, E_M. We define f_{c1} as the frustration where $E_V = E_M$. The upper solid curve in Fig. 8 shows the calculated f_{c1} when only the self-inductance term is included in L, while the lower solid curve shows f_{c1} calculated using the full inductance matrix. Three distinct regions of behavior are distinguishable. In the no-self-field limit, λ much larger than the array size, where λ is the penetration depth appropriate for the system (either $\lambda_\perp$ or λ_J, depending on whether we include all the inductances or just the self-inductance), f_{c1} saturates at a value determined by the system size. At λ on the order of the array size, an increase of f_{c1} is observed as $\lambda_\perp$ decreases, representing the increasing ability of array currents to screen external fields. As $\lambda_\perp$ approaches the lattice spacing, the vortex becomes essentially localized in a single cell, so that further decrease of $\lambda_\perp$ has diminishing influence, and the increase of f_{c1} slows.

We have attempted to obtain analytic forms for f_{c1} in the array by using $H_{c1,L}$, the lower critical field calculated from the London equations for a continuous superconductor of similar size. f_{c1} should be related to $H_{c1,L}$ given by the London solution by

$$f_{c1,L} = \frac{\mu_0 p^2 H_{c1,L}}{\Phi_0} \ . \tag{49}$$

When only the self-inductance is included in the array calculation, we have taken the analogous continuum system of the $N \times N$ array of lattice spacing p to be a cylinder of radius $R = Np/2$. The problem of a vortex located at the center of a cylinder can be solved analytically to give[25]

$$f_{c1,L} = \frac{1}{4\pi\lambda_J^2}\frac{I_0(\frac{R}{\lambda_J})K_0(\frac{\xi}{\lambda_J}) - K_0(\frac{R}{\lambda_J})}{I_0(\frac{R}{\lambda_J}) - 1} \tag{50}$$

where we associate $\xi = p/\sqrt{2\pi}$ as discussed in Ref. 14, and I_0 and K_0 are the modified Bessel functions of the first and second kind, respectively. The calculated $f_{c1,L}$, which is shown as the upper dashed line in Fig. 8, is a good match to the array solution.

No analytic solution is available for the problem of a vortex in a finite thin film. Pearl[10] gives H_{c1} for a vortex in an infinite film, but his result is only valid for $r \gg \lambda_\perp$ and $\lambda_\perp \gg \xi$, and so is not very useful here. Fetter[26] has found a result for H_{c1} applicable for $\lambda \gg R$. In this regime, our numerical result is in good agreement with his calculation, but his solution is inapplicable for $\lambda \ll R$. Therefore, as a check on the array solution, we have used the numerical solution of the Appendix to calculate f_{c1} in a thin disk of radius $R = Np/2$. The result is shown as the lower dashed curve in Fig. 8, and is also seen to be in good agreement with the calculated array solution.

The calculation of f_{c1} clearly illustrates the strong effects of the mutual inductances on the magnetic proper-

ties of vortices in the array, just as the magnetic properties of a thin film are very different from those of a bulk superconductor. In particular, the calculated f_{c1} is much lower when all the mutual inductances are included, representing the importance of long-range interactions, and is very well predicted by a linear model of the superconductor. These results are in contrast to those of Sec. V B, where the energy barrier, a direct result of the nonlinearity of the system, was well predicted by a local model that includes very few of the mutual inductances.

Another way of calculating f_{c1} is by considering the magnetic moment. If we calculate the field H_{c1} at which the energy $-\mu_0 \mathbf{H}_{c1} \cdot \mathbf{M}$ of the vortex magnetic moment $\mathbf{M}$ in the field equals the energy needed to create the vortex,[10] and then obtain f_{c1} from Eq. (49), the computed f_{c1} is the same as in the previously described calculation. The magnetic moment

$$\mathbf{M} = \frac{1}{2} \int dV \, \mathbf{r} \times \mathbf{J} \tag{51}$$

is strongly dependent on the current distribution, which in turn is directly dependent on the form of the inductance matrix, as shown in Sec. V A. The magnetic moment will be higher when all the mutual inductances are included in the calculation, as the currents decay slower than when only a self-inductance term is used to model the induced fields, which explains the lower values of f_{c1}.

VI. CONCLUSION

Self-field effects dramatically alter the properties of vortices in Josephson-junction arrays. Modeling these effects is a difficult numerical problem, and we have presented an efficient algorithm to examine static properties of Josephson arrays.

To describe the current distribution of the vortex in the array, it is necessary to include all the terms in the mutual inductance matrix so that the 3D spatial variance of the magnetic field outside the array is correctly treated. Thus, the magnetic properties of the vortex in an array, which are similar to the magnetic properties of a vortex in a thin film, must be calculated using the full inductance matrix. In order to simulate the arrays using the full inductance matrix, it was necessary to derive a simulation algorithm which exploits a variety of numerical techniques and array properties and is efficient enough to allow simulation of large arrays.

We have shown that the energy barrier increases with decreasing penetration depth (increasing self-field effects), and that to model the energy barrier, the numerical simulation also reveals that it is sufficient to only include self- and nearest-neighbor terms in the inductance matrix. We have presented a simple analytic expression which gives a good fit to the numerically calculated energy barrier.

In addition to the static properties of a vortex placed in the array, one would also like to study the influence of applied magnetic fields and currents. Such a study requires a generalization of the formulation presented herein to use the appropriate thermodynamic potential so that properties such as the depinning current can be found. Our preliminary results show that the depinning current for low magnetic fields is increased beyond $0.1 I_c$ (Ref. 3) as the penetration depth decreases. Due to the increased complexity of formulating applied current in the mesh formulation and the usage of thermodynamic potentials,[27] we have not addressed the case of current-driven arrays here.

The key ideas of the algorithm presented in this paper can be applied to efficient time-dependent simulation of Josephson-junction arrays. Work is in progress on investigating the effect of induced magnetic fields on the *dynamic* properties of vortices in arrays.

ACKNOWLEDGMENTS

We gratefully acknowledge support from NSF Grant No. DMR-9108748 and an IBM equipment grant. J.W. acknowledges support from NSF Grant No. MIP-8858764 A02, and from Defense Advanced Research Projects Agency Contract No. N00014-91-J-1698. J.R.P. acknowledges support from DOD. We would also like to thank K.A. Delin and M. Kamon for useful discussions.

APPENDIX: SOLUTION OF LONDON EQUATIONS IN A DISK

In the London description of a vortex in the center of a disk of radius R, the quantization condition

$$\mu_0 \lambda^2 \oint \mathbf{J} \cdot d\mathbf{l} + \oint \mathbf{A} \cdot d\mathbf{l} = \Phi_0 \tag{A1}$$

must hold for any contour which encloses the vortex. By symmetry $\mathbf{J}$ and $\mathbf{A}$ are circumferentially directed, $\mathbf{J} = J(r)\hat{\phi}$, $\mathbf{A} = A(r)\hat{\phi}$. In a disk of thickness t, with $t \ll \lambda$, the current density will be uniform through the thickness of the disk. Defining the surface current $K_s(r) = tJ(r)$, Eq. (A1) becomes

$$\mu_0 \frac{\lambda^2}{t} K_s(r) + A(r) = \frac{\Phi_0}{2\pi r} \ . \tag{A2}$$

Defining $a(r, r')$ to be the $\hat{\phi}$ component of the vector potential evaluated in the plane of a loop of radius r' carrying unit current, at distance r from the center of the loop, the vector potential $A(r)$ can be written as

$$A(r) = \int_0^R dr' \, K_s(r') a(r, r') \tag{A3}$$

where $a(r, r')$ is given by[28]

$$a(r, r') = \frac{\mu_0}{4\pi} \int_0^{2\pi} \frac{\cos\phi \, d\phi}{[1 + (r/r')^2 - 2(r/r')\cos\phi]^{1/2}} \ . \tag{A4}$$

Substituting Eq. (A3) into Eq. (A2) gives a second-kind integral equation for the surface current $K_s(r)$.

To solve the integral equation numerically, the disk is

discretized into N rings of thickness $dr = R/N$ each of which carries a constant current $K_s(r_i)dr, i = 1 \ldots N$. For purposes of evaluating the vector potential, the rings are considered to have vanishing cross section. For a ring's own contribution to the vector potential at the same r, this prescription is singular, in which case we take the average of the vector potential at points $r+dr/2$, $r - dr/2$. Thus

$$A(r_i) = \sum_{j \neq i} a(r_i, r_j) K_s(r_j) dx + \tfrac{1}{2} K_s(r_i) dx \left[a(r_i + dr/2, r_j) + a(r_i - dr/2, r_j) \right] \ . \tag{A5}$$

The final result is a dense linear system of equations in the N unknowns $K_s(r_i)$ which can be solved by standard techniques. The solutions illustrate the same qualitative features discussed in Sec. (V A) for the Josephson array, in particular the sign change of the field near the edge of the disk, with corresponding increase in $J(r)$.

The field H_{c1} at which it is thermodynamically favorable for a single vortex to exist at the center of the disk occurs when the energy $-\mu_0 \mathbf{H} \cdot \mathbf{M}$ of the vortex magnetic moment $\mathbf{M}$ in the field cancels the energy U_v needed to create the vortex.[10] Thus

$$H_{c1} = \frac{U_v}{\mu_0 M} \ . \tag{A6}$$

Neglecting the contribution of the core ($r < \xi$), the self-energy of the vortex[29] in the disk can be calculated from

$$U_v = \frac{\Phi_0}{2} \int_{\xi}^{R} K_s(r) dr \ . \tag{A7}$$

The magnetic moment is given by

$$\mathbf{M} = \frac{1}{2} \int dV \ \mathbf{r} \times \mathbf{J} \tag{A8}$$

which, for the vortex in a disk where all the currents flow azimuthally, becomes

$$M = \frac{1}{2} \int_{\xi}^{R} r \ K_s(r) \ 2\pi r dr \ . \tag{A9}$$

[1] Physica **B 152**, 1–302 (1988).
[2] C. J. Lobb, D. W. Abraham, and M. Tinkham, Phys. Rev. B **27**, 150 (1983).
[3] M. S. Rzchowski, S. P. Benz, M. Tinkham, and C. J. Lobb, Phys. Rev. B **42**, 2041 (1990).
[4] H. S. J. van der Zant, F. C. Fritschy, T. P. Orlando, and J. E. Mooij, Phys. Rev. Lett. **66**, 2531 (1991).
[5] S. P. Benz and C. J. Burroughs, Appl. Phys. Lett. **58**, 2162 (1991).
[6] K. A. Delin (private communication).
[7] K. Nakajima and Y. Sawada, J. Appl. Phys. **52**, 5732 (1981).
[8] A. Majhofer, T. Wolf, and W. Dieterich, Phys. Rev. B **44**, 9634 (1991).
[9] D. Dominguez and J. V. Jose, Phys. Rev. Lett. **69**, 514 (1992).
[10] J. Pearl, Ph.D. thesis, Polytechnic Institute of Brooklyn, 1965.
[11] G. H. Golub and C. F. V. Loan, *Matrix Computations* (Johns Hopkins University Press, Baltimore, 1989).
[12] C. A. Desoer and E. S. Kuh, *Basic Circuit Theory* (McGraw-Hill, New York, 1969).
[13] As is usual, we neglect the supercurrent contribution (kinetic inductance) to the quantization rule, Eq. (1), by assuming that the lateral dimensions of the bars are much larger than the London penetration depth, so that the current is zero in the center of the bars.
[14] T. P. Orlando, J. E. Mooij, and H. S. J. van der Zant, Phys. Rev. B **43**, 10218 (1991).
[15] K. Nakajima and Y. Onodera, J. Appl. Phys. **49**, 2958 (1978).
[16] Strictly speaking, the assumption of constant current density in the bars contradicts the assumption that the kinetic inductance can be neglected. However, the effect of the current distribution on the computed inductance matrix will be less than the effect of the geometry, and will be negligible for bars separated by more than two or three lattice spacings.
[17] A. E. Ruehli, IBM J. Res. Dev. **16**, 470 (1972).
[18] J. M. Gordon, A. M. Goldman, M. Bhushan, and R. H. Cantor, Jpn. J. Appl. Phys. **26-3**, 1425 (1987).
[19] Y. Saad and M. Schultz, SIAM J. Sci. Statist. Comput. **7**, 856 (1986).
[20] J. Stoer and R. Bulirsch, *Introduction to Numerical Analysis* (Springer-Verlag, New York, 1980).
[21] A. V. Oppenheim and R. W. Schafer, *Discrete-time signal processing* (Prentice-Hall, Englewood Cliffs, 1989).
[22] G. Strang, *Introduction to Applied Mathematics* (Wellesley-Cambridge, Wellesley, 1986).
[23] R. S. Dembo, S. C. Eisenstat, and T. Steihaug, SIAM J. Numer. Anal. **19**, 400 (1982).
[24] P. Brown and Y. Saad, SIAM J. Sci. Statist. Comput. **11**, 450 (1990).
[25] T. P. Orlando and K. A. Delin, *Foundations of Applied Superconductivity* (Addison-Wesley, Reading, 1991).
[26] A. L. Fetter, Phys. Rev. B **22**, 1200 (1980).
[27] J. R. Phillips, H. S. J. van der Zant, J. White, and T. P. Orlando (unpublished).
[28] J. D. Jackson, *Classical Electrodynamics* (Wiley, New York, 1975).
[29] B. B. Goodman and J. Matricon, J. Phys. **27**, C3-39 (1966).